Desalination and Water Treatment
www.deswater.com

doi: 10.5004/dwt.2023.29178

282 (2023) 44–52
January

Experimental research and performance analysis of an improved solar still with a solar concentrator and heat recovery units

Mingxian Chen[a], Yanling Jiang[a], Junming Ruan[b], Geng Wei[a], Hongfei Zheng[b], Zhengliang Li[a,*]

[a]*School of Physics and Electronics, Nanning Normal University, Nanning 530299, China, Tel.: +8618977164860, emails: 541273286@qq.com (Z. Li), 125436526@qq.com (M. Chen), gxjyl@126.com (Y. Jiang), wei_geng@nnnu.edu.cn (G. Wei)*
[b]*School of Mechanical Engineering, Beijing Institute of Technology, Beijing 100081, China, emails: 2685020142@qq.com (J. Ruan), hongfeizh@bit.edu.cn (H. Zheng)*

Received 18 May 2022; Accepted 30 November 2022

ABSTRACT

A conventional solar still is a simple desalination device with convenient operation. However, the low temperature, the solar light loss caused by condensation droplets, and the latent heat dissipation constrain the performance. Aiming at these weaknesses, this paper proposes an improved solar still with a solar concentrator and heat recovery units. A compound parabolic concentrator with mirror focuses is employed to concentrate the solar radiation and thus promote the evaporation temperature. An air blower is used to enhance the evaporation and avoid the vapor condensation occurring at the top glass. In addition, the latent heat released by the vapor condensation preheats the feed seawater, inducing the latent heat recovery. The results of simulating the concentrator show that the reception angle of the concentrator is 30°. The experimental test under the actual weather indicates that 3 h of light is available for the device placed along the north–south direction without tracking the sun. The yield per hour and the total efficiency of the 3-h outdoor test reach 431 g and 41.14%, respectively, showing a good water production performance of the proposed solar still.

Keywords: Solar still; Compound parabolic concentrator; Heat recovery; Enhanced evaporation

1. Introduction

Freshwater scarcity has greatly influenced the human daily life and even the survival. The current trend of water shortage estimates that by 2025, the water scarcity will seriously affect the life of 1.8 billion people and cost many lives in African and Asian countries [1]. Moreover, drinking water is expected to be consumed rapidly due to the foreseen increase in the global population, reaching 9.1 billion in 2050 [2].

Solar thermal desalination is a promising method to provide purified water for human, especially for the people in remote and developing regions where the traditional energies are not sufficiently available. In addition, the solar energy driving the desalination devices has sustainable sources, while zero pollution discharge from solar energy also meets the prospect of the worldwide carbon neutral.

Based on different purification principles, kinds of solar thermal desalination types have been proposed and researched previously, among which the solar still is one of the earliest and simplest types. A solar still involves a top glass cover available for the light incoming, a bottom basin to hold the bulk seawater, and side thermal isolated walls to seal the entire device. The simple structure and the low cost make solar stills available and easy-to-use. However, the low productivity and the energy conversion efficiency of a conventional solar still disappoint the users [3].

* Corresponding author.

In recent decades, promoting productivity and efficiency has always been the research focus. The performance of solar stills can be enhanced to some extent with extra assistant equipment such as solar concentrators [4], collectors [5], condensers [6,7] and fans. Among these extra assistant equipment, solar collection system with heat transfer mediums and long pipes may cause derived heat loss. Therefore, the concept of light concentration and direct heating was proposed by Zhu et al. [8]. A non-tracking solar concentrator with a wide reception angle was employed to promote the evaporation temperature and thus boost the productivity of the solar still. The sunlight is directly concentrated on the bulk water, subsequently inducing the evaporation with high temperature. This approach avoids the heat loss in some solar stills with extra heat collectors and long medium pipes. Similar configurations were also utilized by Wang et al. [9,10]. The prospect of a solar still floating on the sea was achieved in their researches with such a structure. The structure involved two glass to seal an air cavity, thus inducing a high temperature at the bottom glass cover and subsequently forcing the vapor to condense at other positions. This action could avoid the interference of condensation droplets to the incoming light. In addition, the droplet condensation occurring at other walls except the top glass cover makes it convenient to set up heat recovery unis based on the initial device. Zhu et al. [11] also proposed a passive solar concentrated still with heat recovery units by employing the structure mentioned above. Experimental results indicated the enhancement of the distilled yield with the assistant of heat recovery units. However, the yield is still not significantly increased resulting from the energy loss at several optical surfaces.

Recently, a novel research direction of interfacial evaporation has greatly interested researchers [12]. Passive high-efficiency evaporation has been achieved based on thermally-localized solar desalination [13]. However, although multistage latent heat recycling greatly increases the system efficiency, the salt crystallization resulting from the utilization of hydrophilic materials may constrain the sustainability of the device. In addition, the large scale distillation may be hard to realized due to the constrained water absorption capacity of hydrophilic materials utilized.

Conventional solar stills have suffered from the inherent weaknesses such as the interference of condensation droplets to the incoming light and inconvenience for installing heat recovery units. These weaknesses have caused the low productivity. Although efforts are made to overcome the weaknesses, some extra shortcomings have emerged that may constrain the utilization of the improved systems. There is an urgent need to find a solar thermal desalination approach that can not only avoid the optical loss caused by condensation droplets but also suitable for setting heat recovery units. This paper proposes an improved solar still with a solar concentrator and heat recovery units. A compound parabolic concentrator with mirror focuses [14] is employed to promote the evaporation temperature. The circuit air flow enhances the seawater evaporation and force the vapor to condense at another cavity of the device, avoiding the interference of condensation droplets to the incoming light. In the meantime, the feeding seawater could be preheated by the latent heat released from the vapor condensation. Therefore, the proposed solar still overcomes the inherent weaknesses of conventional solar stills, enhances the evaporation, and recovers the condensation latent heat, maximizing the device performance. The aims of this research are as follows: 1. Designing and modeling a matchable concentrator and a suitable system structure; 2. Simulating and analyzing the energy transmission characteristic of the proposed concentrator; 3. Researching and evaluating the system thermal performance under outdoor conditions.

2. System description

2.1. Working principle

The diagram of the proposed solar still with a trough structure is shown in Fig. 1 which contains a compound

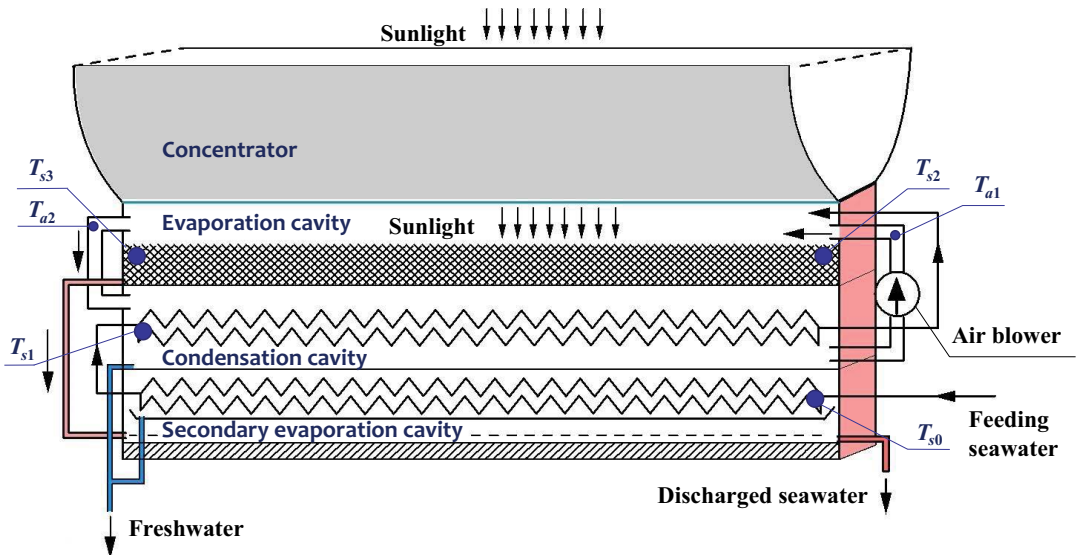

Fig. 1. The diagram of the solar still with a solar concentrator and heat recovery units.

parabolic concentrator with a mirror focus, distillation components, and assistant components. A evaporation cavity, a condensation cavity, and a secondary evaporation cavity locate right below the concentrator from top to bottom. All the three cavities are sealed to form cuboid structures by the glass. A hydrophilic filler is settled at the bottom of the evaporation cavity, while the heat exchangers are put inside the condensation cavity and secondary evaporation cavity, respectively. The assistant components contains a water pump, an air blower, and a feeding water tank. The water pump drives the seawater while the air blower drives the humid air. The detailed working path involves two cycles: the seawater cycle (open) and humid air cycle (closed).

2.1.1. Seawater cycle

At first, seawater is driven by the pump to the heat exchanger in the secondary evaporation cavity from the right inlet. In this heat exchanger, the seawater is preheated by the heat humid air in this cavity at the first time. Then, the seawater goes out of this heat exchanger from the left outlet and enters the heat exchanger of the condensation cavity from the same side. In the heat exchanger of the condensation cavity, the seawater is preheated again by the cycling humid air from the condensation cavity. Next, the seawater leaves the condensation cavity from the right outlet and goes into the evaporation cavity from the same side. In the evaporation cavity, the seawater is absorbed by the hydrophilic fillers, flowing slowly from the right inlet to the left outlet. In the flow process, the seawater is heated by the concentrated solar radiation from the top side. This is the third and the most significant heating of the seawater, while water vapor is produced in this stage. The water vapor evaporated is then involved in the humid air cycle, while the residual concentrated seawater discharged from the left outlet of the evaporation cavity enters the secondary evaporation cavity where the residual seawater evaporates again. The vapor produced here heats the initial feeding seawater in the exchanger locating at the secondary evaporation cavity. The left concentrated seawater is finally discharged from the right side of the secondary evaporation cavity.

2.1.2. Humid air cycle

At the beginning, the humid air is driven into the evaporation cavity by the air blower from the right inlet. The humid air flow then enhances the evaporation of the seawater. Meanwhile, the humid air is heated through the convection with the seawater. Moreover, the water vapor produced goes away with the humid air flow from the left outlet of the evaporation cavity and enters the condensation cavity. The humid air with a high temperature and humidity then exchanges convection heat with the feeding seawater in the exchanger inside the condensation cavity. At the same time, the vapor from the humid air condenses at the surface of the exchanger, releasing heat to the seawater in the exchanger. Next, the humid air leaves the condensation cavity and enters the right inlet of the evaporation cavity to form a cycle.

It is worth mentioning that the humid air cycle occurs only at the evaporation and condensation cavities, while the seawater cycle occurs among all the three cavities. The secondary evaporation cavity is a sealed cavity for gases and an open cavity for the seawater. In addition, there is only the seawater evaporation occurring at the evaporation cavity and only the vapor condensation occurring at the condensation cavity, while both the evaporation and condensation occur at the secondary evaporation cavity.

2.2. Device structure and size

2.2.1. Concentrator

The proposed solar still employs a compound parabolic concentrator with mirror focuses. The working principle of the concentrator is given in Fig. 2 [15]. The concentrator is formed by stretching the 2D section in Fig. 2, which consists of two symmetric parabola sections and secondary reflective mirrors. The secondary reflective mirrors locate below the parabola sections; F_1 and F_2 are the focuses of the two parabolas, respectively; F is the mirror point of F_1 and F_2 about the secondary reflectors.

When the light is in the normal incidence, it would be reflected to the focuses F_1 and F_2 of the two parabolas, respectively. However, due to the existence of secondary reflectors, the light would then be reflected to the mirror focus F.

The inlet width of the concentrator is 385 mm; the outlet width is 85 mm; the height is 418 mm; the stretching length is 1,500 mm; the concentration ratio is 4.53. The coordinate system is established in Fig. 2 with the focus F (0, 36.3),

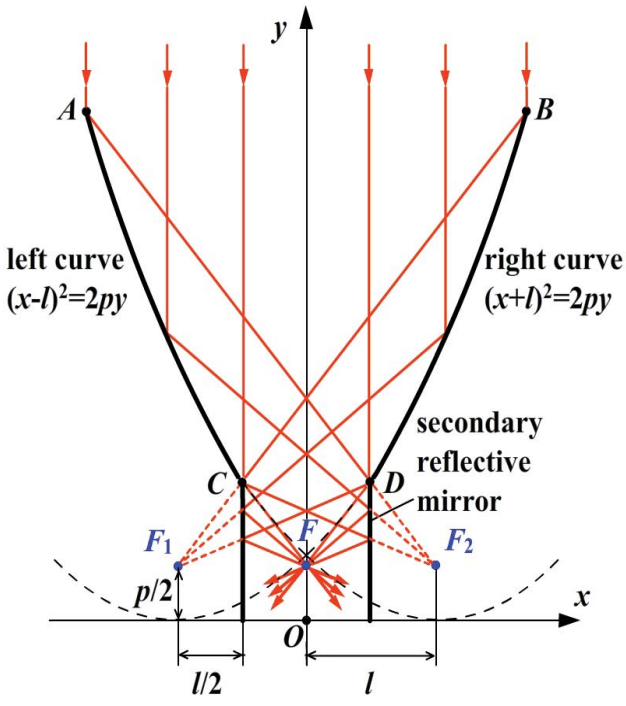

Fig. 2. The working principle of a compound parabolic concentrator with mirror focus.

F_1 (–85, 36.3), F_2 (85, 36.3); the functions of the parabola sections are as follows:

$$\begin{cases} (x-85)^2 = 145.2y, & -192.5 \le x \le -42.5, \text{ section } AC \\ (x-85)^2 = 145.2y, & 42.5 \le x \le 192.5, \text{ section } BD \end{cases} \quad (1)$$

2.2.2. Distillation components

The distillation components locate right below the parabola sections of the concentrator, consisting of the evaporation cavity, the condensation cavity, and the secondary evaporation cavity from the top to the bottom. The top glass cover of the evaporation cavity also serves as the outlet of the parabola sections. The secondary reflectors of the concentrator are embedded in the evaporation cavity to serve as the side walls. All the three cavities are made into the same cuboid structures with length 1,500 mm, width 85 mm, and height 50 mm.

2.3. Experimental tests

The proposed solar still was manufactured according to details in section 2.2. Fig. 3 gives the real photo of the tested device, the air blower, and the pump. The reflective inner layers of the concentrator are reflective aluminum plates; the evaporation cavity, the condensation cavity, and the secondary evaporation cavity are made by transparent glass; the outer walls of the distillation components are attached with thermal insulated layers; spiral copper pipes serve as the heat exchanger in the condensation cavity and the secondary evaporation cavity. Table 1 gives the thermal and optical properties of the construction materials.

The measuring equipment involves: a temperature inspection instrument, thermocouples, a flowmeter, a electronic scale, a solar radiation recorder. The experimental tests were carried out on March 10th and October 15th, respectively, in Beijing (longitude 116°E, latitude 40°N). In the experiments, the device was placed along the north–south line (the stretching direction is parallel with the north–south line); Among the experimental test, salt water with 3.5% salinity was used as the feed seawater to test the thermal characteristic of the solar still; the seawater flux was 5~6.5 kg/h; the cycle air flux was 14~16 m^3/h.

The type, range, resolution, and error of the measuring equipment are given in Table 2. The error of the electronic scale measuring the yield and that of the solar radiation recorder measuring the solar irradiance are 1% and 3%, respectively. According to the error calculation equation (2) [8], the error of the efficiency is 4%, where W is the error with the subscripts m (yield), I (solar irradiance), η (efficiency).

$$W_\eta = \sqrt{\left(\frac{\partial \eta}{\partial m} W_m\right)^2 + \left(\frac{\partial \eta}{\partial I} W_I\right)^2} \quad (2)$$

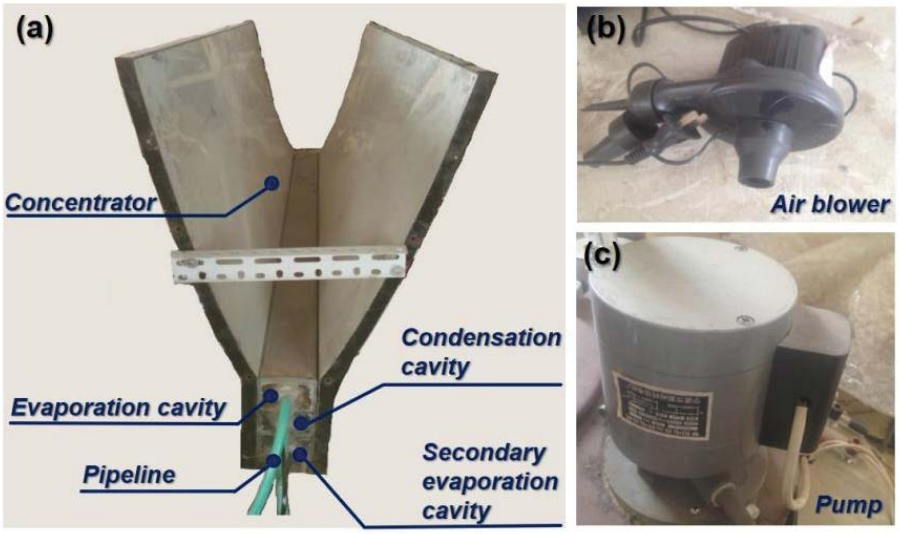

Fig. 3. The real photos of tested device and equipment. (a) The solar still with a solar concentrator and heat recovery units, (b) the air blower and (c) the pump.

Table 1
Thermal and optical properties of the construction materials

Thermal/optical properties	Heat conduction coefficient (W/m·K)		Transmissivity	Reflectivity
Materials	Glass cover	Spiral copper pipes	Glass cover	Reflective aluminum plates
Value	1.03	383	0.91	0.92

Table 2
Type, range, resolution and error of the measuring equipment

Measuring equipment	Range	Resolution	Error (%)
32 channel temperature inspection instrument/ JLS-XMT	–200°C–600°C	0.1°C	1
Electronic scale/HC UTP-06B	0.1–10 kg	0.1 g	1
Solar radiation recorder/TRM-2	0–2,000 W/m^2	1 W/m^2	3
K-type thermocouple	0°C–800°C	0.1°C	1
Salinity meter/Smart AR8012	0–999 ppm	1 ppm	3

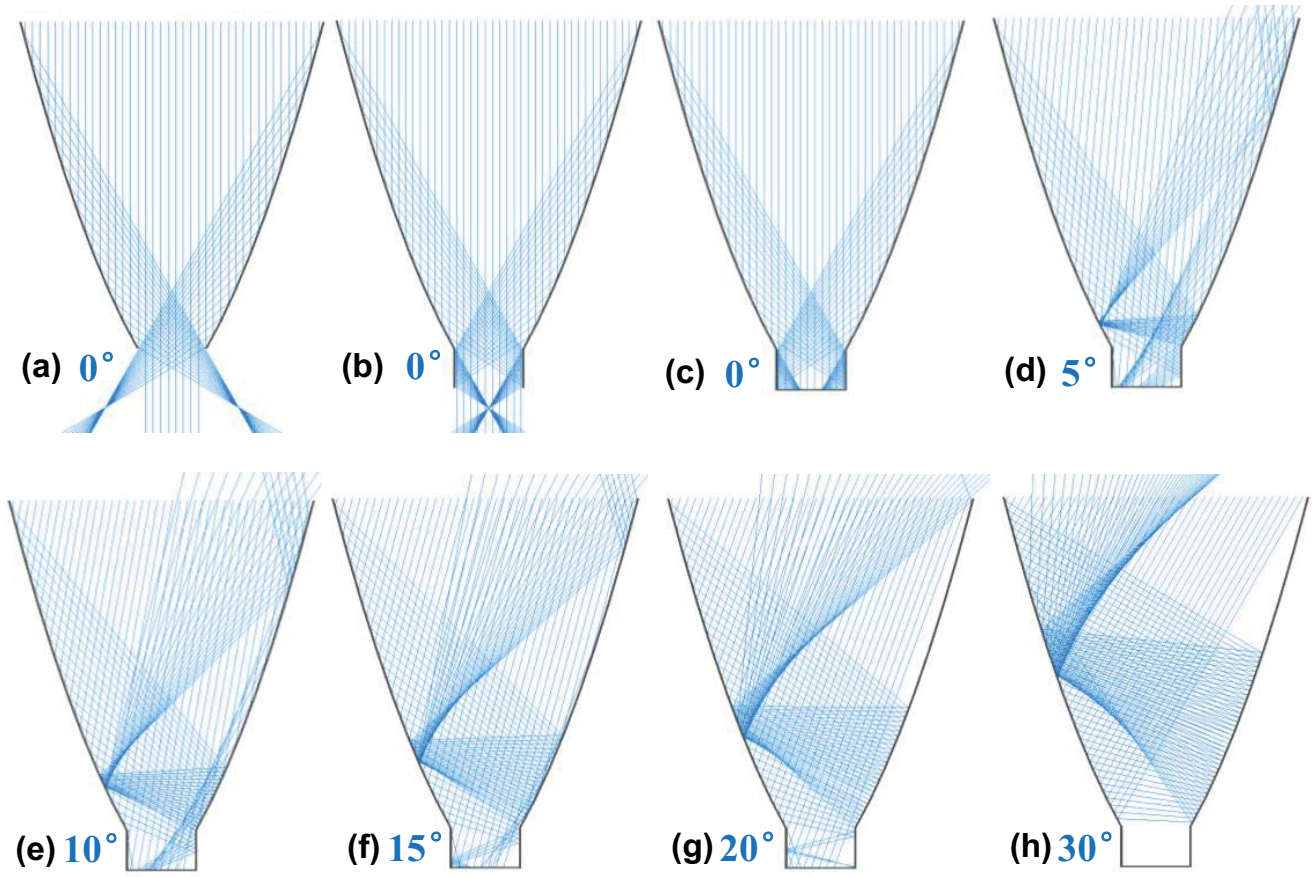

Fig. 4. Light paths under different light incidence angles. (a) Light path of the concentrator with only parabola sections (incidence angle θ = 0°). (b) Light path of the concentrator with secondary reflectors (incidence angle θ = 0°). (c)–(h) Light path of the concentrator with secondary reflectors and a reception surface (incidence angle θ = 0°, 5°, 10°, 15°, 20°, and 30°, respectively).

3. Results and discussion

3.1. Optical simulation

The compound parabolic concentrator with mirror focuses has a good solar concentration performance. This section discusses and analyses the optical performance of the concentrator based on the optical simulation results. The light incidence angle θ is defined as the angle formed by the vertical line and the projection line of the sunlight on the concentrator section surface. Fig. 4a and b are the simulation results of the concentrator without and with secondary reflectors when the light is in the direct incidence (incidence angle θ = 0°). The light is concentrated on the focus of each parabola in Fig. 4a, while the light is reflected to the mirror focus in Fig. 4b due to the secondary reflectors.

Fig. 4c–h represent the light paths within the concentrator with secondary reflectors and a reception surface under the light incidence angle of 0°, 5°, 10°, 15°, 20°, and 30°, respectively. The structure is the configuration of the concentrator and the evaporation cavity employed in the manufactured device. When the light incidence angle is 0°, in Fig. 4c, all the incident light can be absorbed by the reception surface; when the light incidence is 5°, a small

proportion of the incident light cannot be received by the reception surface. On the contrary, the reflected light which cannot pass the outlet of the parabola sections is reflected to the outside from the inlet. With the increase of the incidence angle, as shown in Fig. 4d–g, the light escaping from the inlet increases. Up to 30°, as displayed in Fig. 4h, all the incident light is leaked to the outside from the concentrator inlet, indicating that the reception surface cannot receive the light.

Fig. 5 gives the reception ratio under different light incidence angles, while the reception ratio is defined as the percentage of the light number received by the reception surface to the incident light number. From an overall view, the reception ratio decreases with the increase of the incidence angle. When the incidence angles is >4°, the relationship between the reception ratio and the incidence angle is nearly a line. Moreover, it can be found in Fig. 5 that the reception ratio is 1 when the light incidence angle is 0°, which corresponds with the light path in Fig. 4c; when the incidence angle is 30°, reception ratio is 0, which corresponds with the light in Fig. 4h.

3.2. Results and discussion of the experimental tests

3.2.1. Solar irradiance

Fig. 6 gives the solar irradiance *I*, the solar altitude angle α, the incidence angle θ, and the reception ratio η_r on March 10th and October 15th, respectively. The average solar irradiance is 850 W/m² on March 10th and 1,030 W/m² on October 15th, while the accumulated solar radiation is 5.32 and 6.42 MJ, respectively. The solar altitude angle is from 40° to 45° on March 10th and from 33° to 40° on October 15th. As for the incidence angle, it decreases at the beginning and then increases, while the minimum value 0° appears at the solar noon. The incidence angle of 0° means that the solar light is in the direct incidence direction shown in Fig. 4c. The time of the solar noon (12:27 on March 10th and 12:01 on October 15th) is different for the 2 d resulting from different dates. In addition, from Fig. 6, it is found that the incidence angle is <30° from 11:00 to 14:00 on March 10th and from 11:00 to 13:26 on October 15th, indicating that the solar light could be received by the reception surface in these periods. According to the relationship between the reception ratio and the incidence angle shown in Fig. 5, the reception ratio curves can also be determined as shown in Fig. 5. On both experiment dates, the reception ratio increases at the beginning and then decreases, while the maximum value 1 also occurs at the solar noon. We can find that the tendency of the reception ratio is exactly contrary to that of the incidence angle in Fig. 6 due to their relationship given Fig. 5. Moreover, it is worth mentioning that the reception ratio is 0 after 13:27 on October 15th because the incidence angle is out of the reception range of the concentrator.

3.2.2. Temperature

Fig. 7 gives the temperature of the ambient, the seawater and humid air in different cavities. The average ambient temperature from 11:00 to 14:00 on March 10th and October 15th are 10.3°C and 23.1°C, respectively. The seawater temperature T_{s3} is the maximum among these measuring points. The seawater temperature T_{s2} and T_{s3} both increase at first and then decrease in a similar tendency. The maximum value of T_{s3} is 66.8°C at 12:50 on March 10th

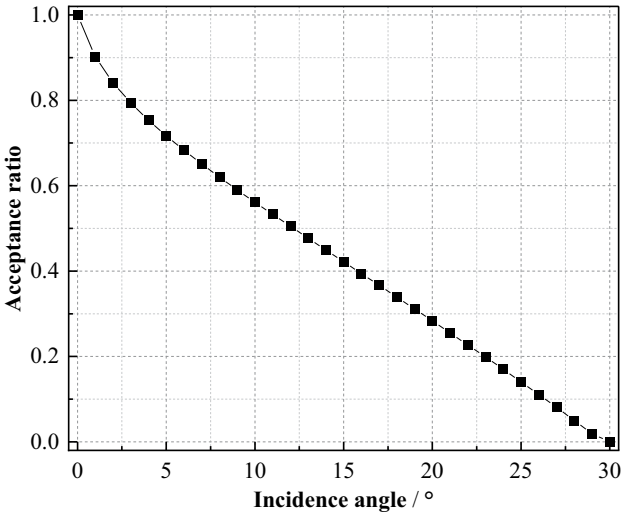

Fig. 5. The reception ratio under different light incidence angles.

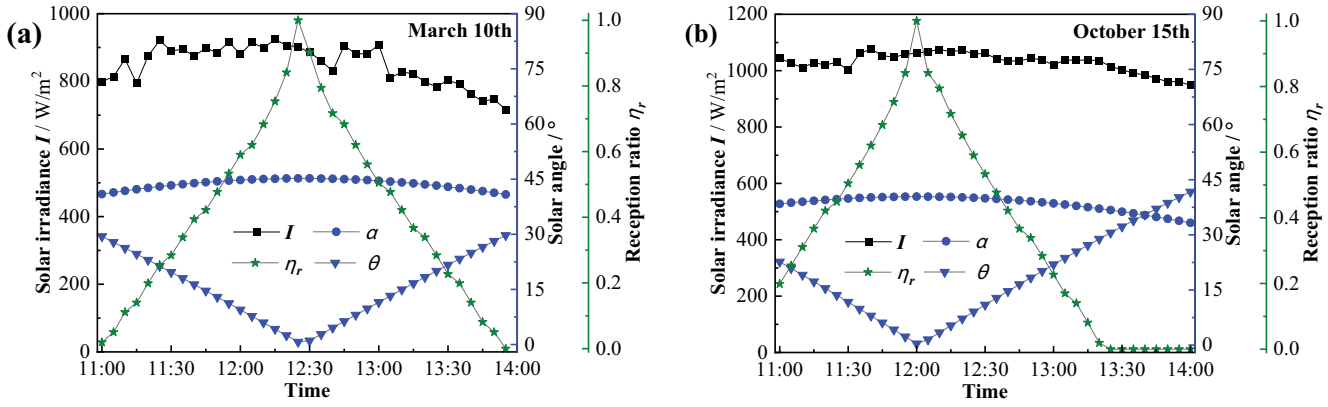

Fig. 6. Solar irradiance, solar angles, and reception ratio.

and 73.8°C at 12:05 on October 15th. The time difference between the peak values of T_{s3} in Fig. 7a and b corresponds to that of the reception ratio in Fig. 6a and b, indicating that the solar noon successively determines the incidence angle, the reception ratio, and the seawater temperature.

As for the humid air, its temperature T_{a2} at the outlet of the evaporation cavity is larger than T_{a1} at the inlet of the evaporation cavity, meaning that the humid air is heated in the evaporation cavity and thus the humidity is promoted. From another viewpoint, in the condensation cavity, the humid air temperature T_{a1} at the outlet is smaller than T_{a2} at the inlet. This is due to the heat exchange between the hot humid air and cold feeding seawater in the condensation cavity. Therefore, the feeding water is heated while the vapor in the humid air also condense to form the fresh water, indicating the latent heat is recovered.

3.2.3. Water yield and efficiency

Fig. 8 gives the results of accumulated solar radiation, freshwater yield and efficiency. According to the reception angle range, the experiments were carried out from 11:00 to 14:00, while the freshwater yield is measured per hour. The water production efficiency is calculated as Eq. (3).

$$\eta = \frac{M_e h_{fg}}{\sum IA} \tag{3}$$

where M_e is the yield; h_{fg} is the latent heat of water vapor; I is the solar irradiance; A is the area of the concentrator inlet.

From Fig. 8, the total freshwater yield and efficiency on October 15th were more than that on March 10th due to more accumulated solar radiation on October 15th. As for the hourly yield on October 15th, 431 g freshwater was produced from 11:00 to 12:00, which was more than the yield in the other two periods. The freshwater yield corresponded with the peak seawater temperature occurring at 12:00 in Fig. 7b. By comparison, the peak seawater temperature occurred after 12:00 on March 10th, resulting in less hourly yield from 11:00 to 12:00 than the other two periods. The total efficiency were 35.13% on March 10th and 41.14% on October 15th, respectively, indicating that the performance of the proposed solar still was satisfying.

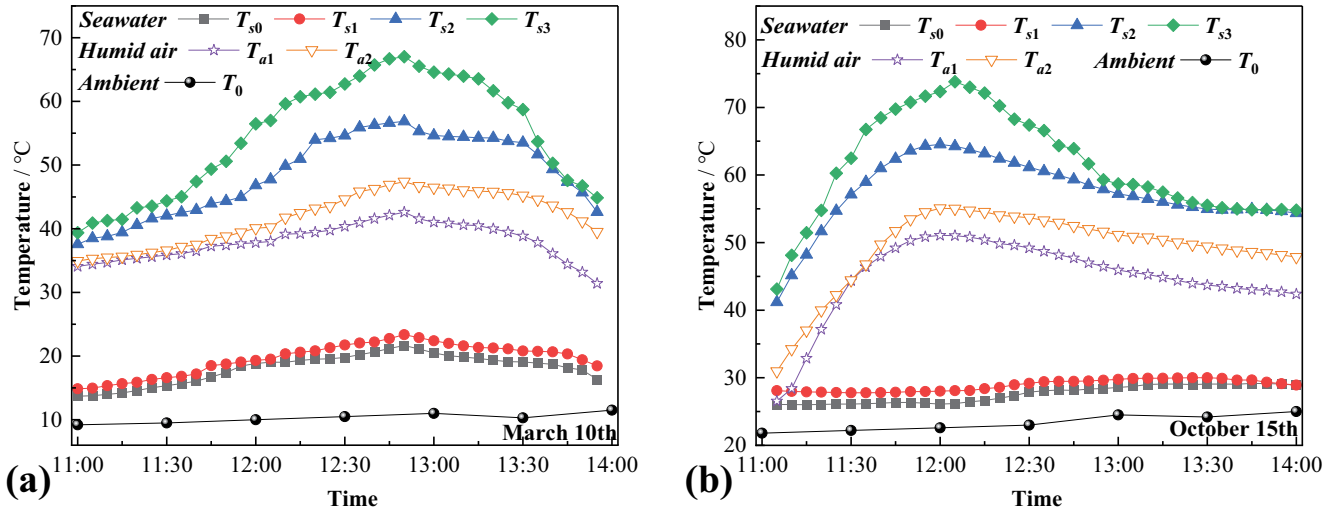

Fig. 7. Temperatures of the ambient, seawater and humid air.

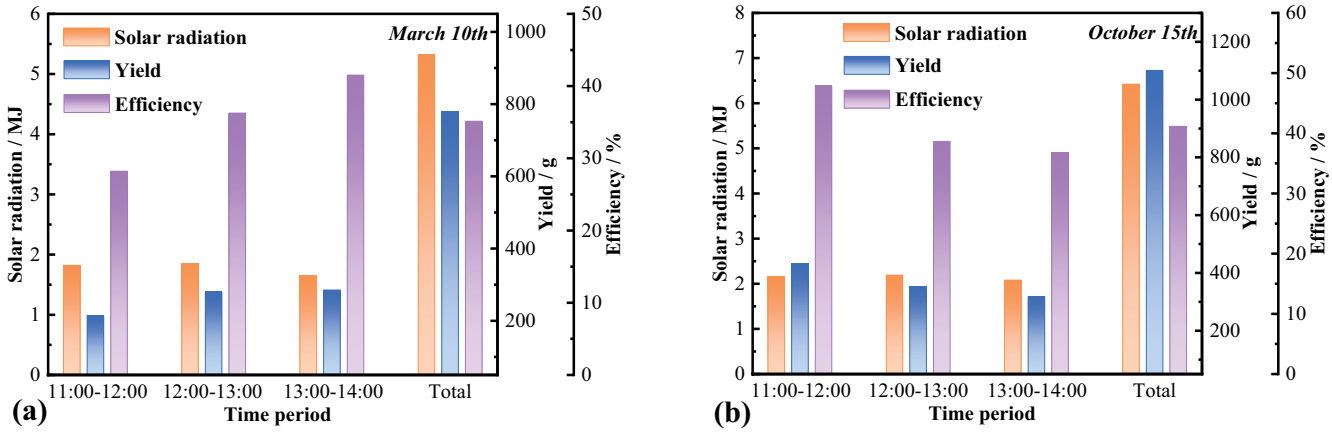

Fig. 8. Experimental radiation, yield, and efficiency.

Fig. 9 gives the salinity of the feed water and distilled water. The salinity of the feed water is 3.5% before distillation, and of 45 ppm/50 ppm on March 10th/October 15th, which is less than the salinity standard (200 ppm) of WHO, showing a good water quality using the approach proposed.

3.3. Comparison with the research in the literature

This research proposes a new solar thermal desalination approach that can not only avoid the optical loss caused by condensation droplets but also suitable for setting heat recovery units. At the same time, multistage evaporation is also achieved in the structure employed to boost the yield. Table 3 gives the test results of different solar stills with concentrators. The water production efficiency (above 40%) in this study is comparative among the same types of solar stills, which expresses the application potential of the present design in the future.

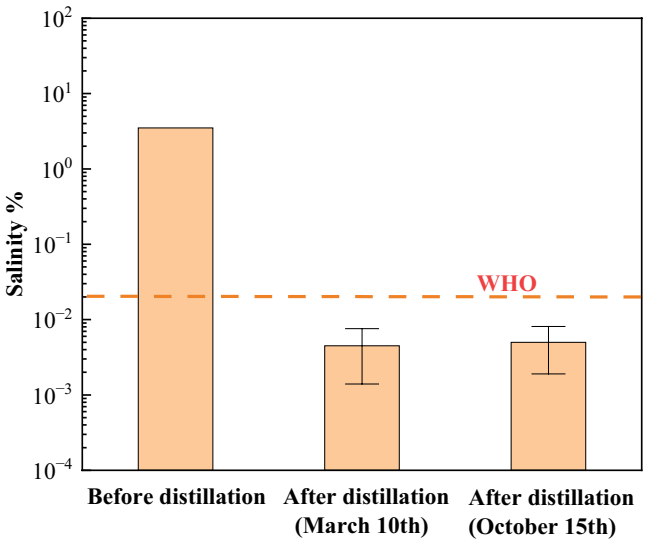

Fig. 9. Salinity of the feed water/distilled water before and after distillation.

3.4. Economic analysis

Table 4 gives the cost of the solar still components. The total fixed cost (C_F) of the manufactured solar still with assistant equipment is 39.1 \$. We assume that the solar still can serve for n (n = 15) years with the annual maintenance cost (C_A) 5 \$. Therefore, the total cost (C_T) for the life time of the solar still is calculated as 114.1 \$ by Eq. (4). If we assume the solar still works for m days (m = 335) per year with the total daily radiation G (G = 2.5 × 10^4 kJ/m^2) and average efficiency η (η = 40%), the total water yield M (kg) for the life time is calculated as by Eq. (5), where A is the solar concentrator aperture area, h_{fg} is the evaporation latent heat. Therefore, the distilled freshwater price (P_D) is 0.0094 \$/kg by Eq. (6). In addition, we assuming the sale price of the freshwater (P_S) is 0.07 \$/kg (lower than the sale price of the pure water in the market) [18], the payback period (PP) of the total cost is about 2.02 y, based on Eq. (7).

$$C_T = C_F + n \times C_A \tag{4}$$

$$M = \frac{Anm\eta G}{h_{fg}} \tag{5}$$

Table 4
Cost of solar still components

Components	Cost (\$)
Heat exchanger	17.7
Water pump	8.5
Air blower	7.1
Glass cover and supporter	2.5
Reflective aluminum plates	1.4
Pipelines and other consumable items	1.9
Total	39.1

Table 3
Performance comparison with the research in the literature

Research	Author and references	Water yield per unit aperture solar collector area (kg/m^2)	Total solar incident radiation (MJ/m^2)	Efficiency (%)
Solar desalting system with a parabolic concentrator	Arunkumar et al. [16]	1.95	24.6	19.0
Tubular solar still with a parabolic concentrator	Elashmawy [17]	3.53	28.2	30.0
Solar still with a compound parabolic concentrator	Zhu et al. [8]	2.95	24.5	28.9
		2.24	23.1	23.2
Floating solar still with a compound parabolic concentrator	Wang et al. [10]	1.38	17.2	19.3
		1.19	12.6	22.7
Solar still with a compound parabolic concentrator and heat recovery units	Zhu et al. [11]	3.67	23.33	37
This study	Chen et al.	1.35	9.2	35.1
		1.9	11.1	41.1

$$P_D + \frac{C_T}{M} \tag{6}$$

$$PP = \frac{n \times C_T}{P_S \times M} \tag{7}$$

4. Conclusion

Low temperature, solar energy loss caused by condensation droplets, and dissipation of the latent heat constrain the performance of a solar still. To improve the performance, this paper proposes an improved solar still with a solar concentrator and heat recovery units. A compound parabolic concentrator with mirror focuses is employed to concentrate the solar radiation and thus to promote the evaporation temperature. An air blower is used to enhance the evaporation and avoid the vapor condensation at the top glass. In addition, the latent heat released by the vapor condensation preheats the feed seawater, realizing the latent heat recovery.

The proposed concentrator is designed and simulated in this paper, while the results show that the reception angle of the concentrator is 30°. The experimental test under the actual weather indicates that 3 h of light is available without tracking the sun. The yield per hour and the total efficiency of the 3-h outdoor test reaches 431 g and 41.14%, respectively, showing a good water production performance of the proposed solar still.

This paper proposes the concept of a novel solar concentrated still and carries out initial experimental test for the manufactured device. In the future, the water production performance could be further researched under the condition of tracking the sun throughout the day. In addition, the impact of the concentration ratio, seawater flux, and air flux could be also studied.

Acknowledgments

This work is supported by Guangxi Natural Science Foundation (No. 2018GXNSFAA050139, No. 2020GXNSFAA297184).

References

[1] M. Mohsenzadeh, L. Aye, P. Christopher, Development and experimental analysis of an innovative self-cleaning low vacuum hemispherical floating solar still for low-cost desalination, Energy Convers. Manage., 251 (2022) 114902, doi: 10.1016/j.enconman.2021.114902.

[2] D. Purnachandrakumar, G. Mittal, R.K. Sharma, D.B. Singh, S. Tiwari, H. Sinhmar, Review on performance assessment of solar stills using computational fluid dynamics (CFD), Environ. Sci. Pollut. Res., 29 (2022) 38673–38714.

[3] F.A. Essa, Thermal Desalination Systems: From Traditionality to Modernity and Development, V. Steffen, Ed., Distillation Processes, InTechOpen, London, 2022, doi: 10.5772/intechopen.101128.

[4] D. Singh, S. Gautam, A. Kumar, Analytical study of photovoltaic thermal compound parabolic concentrator active double slope solar distiller with a helical coiled heat exchanger using CuO nanoparticles, Desal. Water Treat., 233 (2021) 30–51.

[5] R. Kumar, D.B. Singh, A. Dewangan, V.K. Singh, N. Kumar, Performance of evacuated tube solar collector integrated solar desalination unit-a review, Desal. Water Treat., 230 (2021) 92–115.

[6] M. Al-Dabbas, A. Alahmer, A. Mamkagh, M.R. Gomaa, Desalination and water treatment productivity enhancement of the solar still by using water cooled finned condensing pipe, Desal. Water Treat., 213 (2021) 35–43.

[7] F.A. Essa, W.H. Alawee, S.A. Mohammed, A.S. Abdullah, Z.M. Omara, Enhancement of pyramid solar distiller performance using reflectors, cooling cycle, and dangled cords of wicks, Desalination, 506 (2021) 115019, doi: 10.1016/j.desal.2021.115019.

[8] Z. Zhu, H. Zheng, Q. Wang, M. Chen, Z. Li, B. Zhang, The study of a novel light concentration and direct heating solar distillation device embedded underground, Desalination, 447 (2018) 102–119.

[9] Q. Wang, Z. Zhu, G. Wu, X. Zhang, H. Zheng, Energy analysis and experimental verification of a solar freshwater self-produced ecological film floating on the sea, Appl. Energy, 224 (2018) 510–526.

[10] Q. Wang, Z. Zhu, H. Zheng, Investigation of a floating solar desalination film, Desalination, 447 (2018) 43–54.

[11] Z. Zhu, Q. Wang, Z. Li, M. Chen, L. Wang, H. Zheng, Performance research and comparison of integrated passive solar-concentrated stills buried in soil: with/without heat recovery, Energy Convers. Manage., 256 (2022) 115400, doi: 10.1016/j.enconman.2022.115400.

[12] P. Tao, G. Ni, C. Song, W. Shang, J. Wu, J. Zhu, G. Chen, T. Deng, Solar-driven interfacial evaporation, Nat. Energy, 3 (2018) 1031–1041.

[13] L. Zhang, Z. Xu, L. Zhao, B. Bhatia, Y. Zhong, S. Gong, E.N. Wang, Passive, high-efficiency thermally-localized solar desalination, Energy Environ. Sci., 14 (2021) 1771–1793.

[14] H. Zheng, C. Feng, Y. Su, R. Wang, X. Xue, Performance analysis and experimental investigation of a novel trough daylight concentration and axial transmission system, Sol. Energy, 97 (2013) 200–207.

[15] T. Tao, Z. Hongfei, H. Kaiyan, A. Mayere, A new trough solar concentrator and its performance analysis, Sol. Energy, 85 (2011) 198–207.

[16] T. Arunkumar, D. Denkenberger, R. Velraj, R. Sathyamurthy, H. Tanaka, K. Vinothkumar, Experimental study on a parabolic concentrator assisted solar desalting system, Energy Convers. Manage., 105 (2015) 665–674.

[17] M. Elashmawy, An experimental investigation of a parabolic concentrator solar tracking system integrated with a tubular solar still, Desalination, 411 (2017) 1–8.

[18] Y. Zhao, O. Ramadan, H. Kong, X. Xue, S. Riffat, H. Zheng, Performance analysis and optimization of a novel high-efficiency flower-inspired solar still, Energy Convers. Manage., 251 (2022) 114878, doi: 10.1016/j.enconman.2021.114878.